Available online at www.sciencedirect.com

ScienceDirect

www.elsevier.com/locate/jes

JES JOURNAL OF ENVIRONMENTAL SCIENCES

www.jesc.ac.cn

Influence of particle size on the aggregation behavior of nanoparticles: Role of structural hydration layer

Hongyan Sun[1,2,3], *Ruyuan Jiao*[1,2,*], *Guangyu An*[1,2], *Hui Xu*[1,2], *Dongsheng Wang*[1,2,3,*]

[1] *State Key Laboratory of Environmental Aquatic Chemistry, Research Center for Eco-Environmental Sciences, Chinese Academy of Sciences, Beijing 100085, China*
[2] *Key Laboratory of Drinking Water Science and Technology, Research Center for Eco-Environmental Sciences, Chinese Academy of Sciences, Beijing 100085, China*
[3] *University of Chinese Academy of Sciences, Beijing 100049, China*

ARTICLE INFO

Article history:
Received 18 June 2020
Revised 10 October 2020
Accepted 11 October 2020
Available online 24 October 2020

Keywords:
Nanoparticles
Particle size
Aggregation rate coefficient
Structural hydration layer
Derjaguin, Landau, Verwey and Overbeek (DLVO) theory

ABSTRACT

More and more attention has been paid to the aggregation behavior of nanoparticles, but little research has been done on the effect of particle size. Therefore, this study systematically evaluated the aggregation behavior of nano-silica particles with diameter 130–480 nm at different initial particle concentration, pH, ionic strength, and ionic valence of electrolytes. The modified Smoluchowski theory failed to describe the aggregation kinetics for nano-silica particles with diameters less than 190 nm. Besides, ionic strength, cation species and pH all affected fast aggregation rate coefficients of 130 nm nanoparticles. Through incorporating structural hydration force into the modified Smoluchowski theory, it is found that the reason for all the anomalous aggregation behavior was the different structural hydration layer thickness of nanoparticles with various sizes. The thickness decreased with increasing of particle size, and remained basically unchanged for particles larger than 190 nm. Only when the distance at primary minimum was twice the thickness of structural hydration layer, the structural hydration force dominated, leading to the higher stability of nanoparticles. This study clearly clarified the unique aggregation mechanism of nanoparticles with smaller size, which provided reference for predicting transport and fate of nanoparticles and could help facilitate the evaluation of their environment risks.

Introduction

Solid particles are ubiquitous in aquatic environments, including natural minerals, metal oxides and carbon materials (Ivanić et al., 2020; Zaouri et al., 2017; Zhang et al., 2019). Among them, nanoparticles attract more and more attention because of their unique nature. Due to smaller size and larger specific surface area, nanoparticles are prone to adsorb heavy metals, pesticides, polycyclic aromatic hy-

* Corresponding authors at: State Key Laboratory of Environmental Aquatic Chemistry, Research Center for Eco-Environmental Sciences, Chinese Academy of Sciences, Beijing 100085, China.
E-mails: ryjiao@rcees.ac.cn (R. Jiao), wgds@rcees.ac.cn (D. Wang).

https://doi.org/10.1016/j.jes.2020.10.007
1001-0742/

drocarbons, polychlorinated biphenyls and natural organic matters (Adeleye et al., 2018; Liu et al., 2018; Wang et al., 2018; Zhang et al., 2020), which cannot only reduce biological degradation rates of the hazardous pollutants, but also affect the bioavailability and toxicity of the pollutants to aquatic organisms (Combarros et al., 2016; Liu et al., 2019). Moreover, nanoparticles can be ingested mistakenly by various aquatic organisms, such as fungi, shrimp and zebrafish, leading to growth inhibition, morphological abnormalities and even mortality (Kansara et al., 2019; Lish et al., 2019; Wang et al., 2020). Therefore, it is imperative to explore the transport and behavior of nanoparticles in aquatic environments.

Nanoparticles would inevitably undergo aggregation once released into aquatic environments due to Brownian motion, which could directly influence their environment fate and ecological risks (Yan et al., 2019). It was reported that the aggregate size of nanoparticles could influence the bioavailability to microorganisms and the sorption capacity for organic contaminants (French et al., 2009; Zhang et al., 2013). The collisions between nanoparticles yield primary flocs, whose morphology and structure impact the treatment efficiency of coagulation and membrane processes (Chekli et al., 2013; Jarvis et al., 2005). Hence, the aggregation behavior and stability of nanoparticles should be investigated. In general, the stability of colloidal suspension is characterized by the classical theory of Derjaguin, Landau, Verwey and Overbeek (DLVO) (Derjaguin and Landau, 1941; Verwey and Overbeek, 1948). The DLVO theory considered particle interaction as a superposition of inter-particle electrostatic repulsion and van der Waals (vdW) attraction, which successfully interpreted the aggregation behaviors of colloidal particles in aquatic environments. The critical coagulation concentration (CCC) divided the aggregation process into two regimes, namely slow aggregation regime and fast aggregation regime (Russel et al., 1989). Later, the Smoluchowski theory was used to describe the kinetic process between two spherical particles in the fast aggregation regime, in which the surface charges were screened off by highly concentrated electrolyte ions with the vdW attraction being the only interaction force (Derjaguin, 1940). Based on the theory, the fast aggregation rate coefficient was predicted to be a constant (6.16×10^{-18} m^3/sec at temperature (T) = 25°C), independent of particle size, solution pH and other parameters (Von Smoluchowski, 1917). However, subsequent researches discovered that the real aggregation rate coefficients were approximately half of the theory's prediction (Holthoff et al., 1996; Zhou et al., 2014). This discrepancy were successfully explained by the modified Smoluchowski theory, which incorporated hydrodynamic resistances into the inter-particle interaction force besides electrostatic repulsion and vdW attraction. The fast aggregation rate coefficient predicted by the modified Smoluchowski theory was revised as 3.49×10^{-18} m^3/sec (at T = 25°C), which was still independent of particle size and solution chemistry (Honig et al., 1971; Spielman, 1970).

Nevertheless, the modified Smoluchowski theory was noted to fail to predict the fast aggregation rate coefficient of nanoparticles under certain circumstances. For instance, Higashitani et al. (2017) experimentally confirmed that the fast aggregation rate coefficients of nano-silica with different diameters were affected by particle sizes. When the particle size was less than 300 nm, the nanoparticles would experience fast aggregation rate coefficient deviating from the modified Smoluchowski theory, with the deviation being greater at the smaller particle size. In particular, the 50 nm nano-silica would have a fast aggregation rate coefficient four orders of magnitude lower than the theoretical prediction. A study by Kobayashi et al. (2005) showed that the fast aggregation rate coefficients of 30–80 nm silica particles depended not only on particle size but also on solution's pH and ionic strength. It was revealed that the coefficient was a constant at pH 6-12 but was a function of pH at other conditions. The anomalous variations of fast aggregation rate coefficient were also reported in other studies (Adachi et al., 1994).

Previous investigations indicated that nanoparticles would have unique aggregation mechanism when the particle size below a certain value, but the reason was not elucidated clearly. Therefore, it is necessary to explore the impact of particle size on nanoparticles' aggregation behavior. However, to the best of authors' knowledge, limited information has been reported. Although direct surface force measurement confirmed the presence of a structural hydration layer on the mineral surface (Kilpatrick et al., 2013; Reischl et al., 2019), its affection on the mineral particles with different sizes is still unavailable. Moreover, how the structural hydration layer thickness changes with the external conditions also remains ambiguous.

Therefore, nano-silica was selected as a model mineral nanoparticles due to its universality and spherical shape (Liu et al., 2011). This study performed systematical investigation on aggregation behavior of nano-silica with diameters 130–480 nm at pH 9-11 under different initial particle concentration, ionic strength and ionic valence of electrolytes. Through comparing variation of aggregation rate coefficients under different conditions, the formation mechanism of structural hydration layer was explored. Considering the repulsion of structural hydration layer, a new model was established based on the modified Smoluchowski theory. Based on the model, the thickness of structural hydration layer as a function of particle size was acquired and the effect of pH and cation species on fast aggregation rate coefficients were successfully interpreted. By comparing the thickness of structural hydration layer and the distance at the primary minimum, the unique aggregation mechanism of nanoparticles was illuminated. This study provided theoretical foundation for assessing transformation, fate and the ecological risks of nanoparticles in aquatic environments.

1. Materials and methods

1.1. *Chemicals*

Sodium hydroxide (NaOH), hydrochloric acid (HCl), sodium chloride (NaCl), barium chloride dihydrate ($BaCl_2 \cdot 2H_2O$) and lanthanum (III) chloride hydrate ($LaCl_3 \cdot xH_2O$) were all obtained from Sinopharm Chemical Reagent Co., Ltd., China. NaCl (4 mol/L), 20 mmol/L $BaCl_2 \cdot 2H_2O$ and 10 mmol/L $LaCl_3 \cdot xH_2O$ were prepared as stock solutions. All the reagents used in this study were analytical grade and Milli-Q water was used to be the solvent in all solutions.

1.2. *Preparation of silica suspensions*

Nano-silica was purchased from Aladdin, China. The density of the silica particles, provided by producer, is 2.2 g/cm^3. Many articles directly bought silica suspensions with different diameters from the manufacturers, which could inevitably have the influence of surfactants. Therefore, in this study, a natural way of hydraulic screening was used to obtain different size distribution of silica suspensions. Nano-silica (25 g) was dispersed in 5 L deionized (DI) water in a high-speed blender. After blending at 4000 r/min for 30 min, various volume of 1 mol/L NaOH was added to the solution to increase the dispersion of nanoparticles and stirred magnetically for one day. According to the Stokes formula, the sedimentation speed of particles with different diameters are diverse (Miyahara et al., 2002). Therefore, after different days' sedimentation, the supernatant at different heights was decanted and retained. For example, a 130 nm diameter particle would settle 10 mm for 10 days while a 480 nm diameter particle would settle about 26 mm for 2 days. Its solid content was measured by gravimetry method (Sun et al., 2019) and the volume average diameters of particles were measured by dynamic light scattering (DLS, Zetasizer Nano ZS90, Malvern, UK). Using this method, eight kinds of nano-silica suspensions with different particle diameters (130, 140, 150, 160, 190, 270, 330 and 480 nm) were obtained. The size distribution of the eight suspensions were shown in Appendix A Fig. S1. The polydispersity index (PDI) of the eight suspensions were around 0.10, respectively. Since the difference of PDI is not significant, the influence of dispersion on the aggregation rate coefficient could be excluded (Zhang et al., 2011).

1.3. *Aggregation kinetics*

Lips and Willis (1973) developed a method to determine the value of absolute aggregation rate coefficient of monodisperse spherical sols by using low angle light scattering technique. Mie functions and Rayleigh–Gans–Debye (R-G-D) theory were used to describe the light scattering properties of single spheres and an inter-particle interference term, respectively. It was found that the intensity of scattered light was independent of the shape of aggregates when the scattering angle was near zero. Therefore, the change in the intensity of scattered light at a low angle was increased linearly with time and further an unambiguous value of the coagulation rate coefficient could be obtained from the measurement of the slope, as shown in the following equation.

$$(I(t) - I(0))/I(0) = 2KN_0t \quad (1)$$

where $I(t)$ (cd) and $I(0)$ (cd) is the intensity of scattered light at time t and 0, K (m^3/sec) is the value of aggregation rate coefficient, N_0 (particles/m^3) is the total initial number concentration of particles, which is determined by the particle size and the dry weight of particles in suspensions and t (sec) is the elapsed time.

A laser diffraction instrument (Mastersizer 2000, Malvern, UK) operating with a He–Ne laser at a wavelength of 633 nm was used to detect the change of scattered light intensity at the scattering angle of 0.0144°. Only the early stage aggregation kinetics was evaluated by measuring the initial rate at which scattered light intensity varies over time. One of the result was set as an example and shown in Fig. S2. The scattered light intensity did change linearly with time. With increasing the ionic strength, the slope increased as well.

Equal volume of silica and electrolyte solutions were filled in 100 ml glass beaker and then pumped into the Mastersizer through optical unit and then backed to the beaker by a peristaltic pump. Intensity measurements were taken every 6 sec for the duration of aggregation. A small sample was taken immediately after 2 min mixing for the determination of zeta potential (Zetasizer Nano ZS90, Malvern, UK). Parallel experiments with at least three times were took out to avoid the occurrence of errors. All the tests were conducted at 25°C.

2. Results and discussion

2.1. *Effect of particle size on fast aggregation rate coefficients*

Fig. 1 shows the aggregation rate coefficients for nano-silica with different particle sizes at high (1.85 × 10^{17} particles/m^3) and low (1.85 × 10^{16} particles/m^3) initial particle concentra-

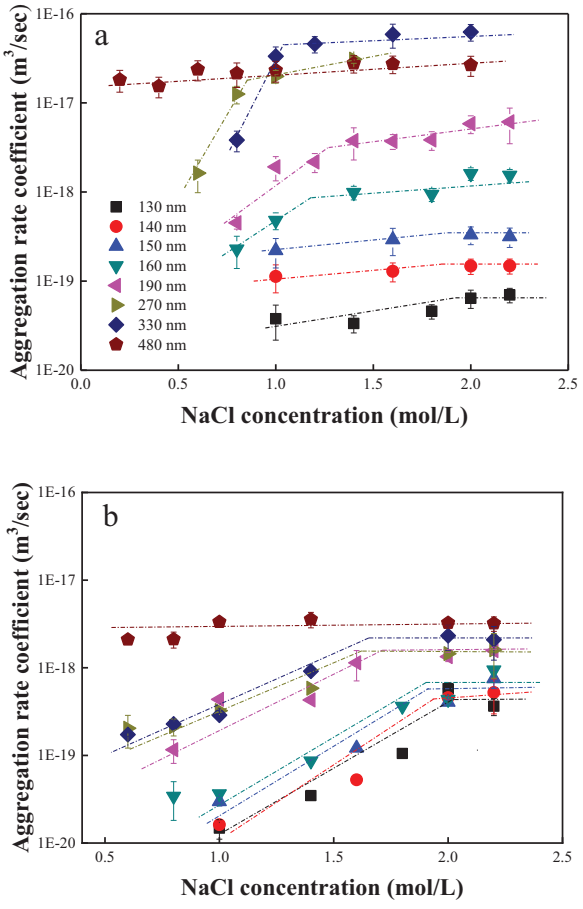

Fig. 1 – Aggregation rate coefficients for silica of different diameters as a function of NaCl concentration at pH 10 with initial particle concentration of (a) 1.85 × 10^{17} particles/m^3 and (b) 1.85 × 10^{16} particles/m^3.

tions. No aggregation was occurred at pH inferior to 9, so the pH was set at 10 herein. The details of the pH effect would be discussed in Section 2.4. At high initial particle concentration (Fig. 1a), the aggregation rate coefficients were increased with ionic strength until the ionic strength reached the CCC. This finding conformed to the DLVO theory that assumed an electrolyte-stimulated aggregation transformed from the slow regime to the ultimate fast regime at CCC. As shown in Fig. S3, in the slow aggregation regime, electrostatic repulsion played a dominant role, preventing particles from colliding with each other. As the electrolyte concentration increased, the charges on particles' surfaces were neutralized and the electrostatic repulsion was almost shielded in the fast aggregation regime. However, as the particle size reduced, the transition became unconspicuous, which meant the DLVO theory might not be able to comprehensively describe the stability of nanoparticles with smaller size. In addition, with the decrease of the particle size, the value of CCC increased gradually. The forementioned phenomena were also discovered at low initial particle concentration (Fig. 1b). Comparing the effect of ionic strength variation on aggregation rate coefficients, at low ionic strength (1 mol/L NaCl), the aggregation rate coefficients of all particle sizes at low initial particle concentration were all lower than that at high initial particle concentration. While at high ionic strength (2.2 mol/L NaCl), only the particles with size over 190 nm presented less fast aggregation rate coefficients than that at high initial particle concentration. This observation indicated that both the particle size and particle concentration significantly affected aggregation rate coefficients in the reaction-controlled regime; but the former predominated aggregation process in the diffusion-controlled regime.

The fast aggregation rate coefficients of nano-silica particles with different diameters in 2.2 mol/L NaCl solution at pH 10 were shown in Fig. 2. It was obvious that both the Smoluchowski theory (Derjaguin, 1940) and the modified Smoluchowski theory (Spielman, 1970) failed to describe the aggregation kinetics for the studied nano-silica particles. Hatton et al. (1974) also discovered the similar result. At high initial particle concentration (green rectangle in Fig. 2), the fast aggregation rate coefficients were higher than the theory value (3.49×10^{-18} m^3/sec) at particle size over 190 nm. The classical Smoluchowski theory was used to describe the collision process between two spherical particles in a dilute solution (Adachi et al., 1994). Therefore, as the solution concentration increased to a certain level, multi-collisions among particles of various sizes or the collisions between clusters could occur even in the early state of coagulation, resulting in the higher aggregation rate coefficient (Hatton et al., 1974). The similar finding has also been discovered by Adachi (1995) that as the initial particle concentration higher than 10^{14} particles/m^3, the aggregation rate coefficient was higher than the theory value. Conversely, at particle size below 190 nm, the fast aggregation rate coefficient was lower than the theory, and the degree of deviation increased with the decrease of particle size. At 130 nm particle size, the aggregation rate coefficient was one order of magnitude lower than the theoretical prediction value. At low initial number concentration (red cycle in Fig. 2), the fast aggregation rate coefficients with particle size larger than 190 nm were consistent with the modified Smoluchowski theory values. However, deviation also occurred as the particle size was less than 190 nm.

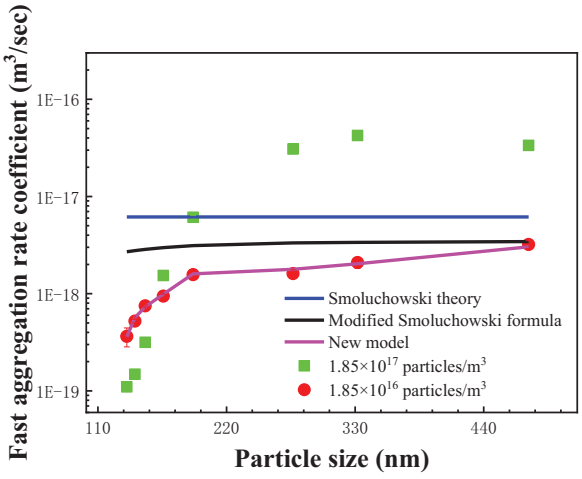

Fig. 2 – Fast aggregation rate coefficient as a function of particle size. Silica particles in 2.2 mol/L NaCl solution at pH 10. Blue solid line: K_R (fast aggregation rate coefficient) from Smoluchowski theory; Black solid line: K_R from modified Smoluchowski theory; Carmine solid line: K_R fitted by the new model; Green rectangle and red cycle: initial particle concentration of 1.85×10^{17} and 1.85×10^{16} particles/m^3, respectively.

In brief, the modified Smoluchowski theory failed to describe the aggregation kinetics for nano-silica particles with diameter less than 190 nm regardless of the initial particle concentration. There must be additional repulsive forces causing the fast aggregation rate coefficient to deviate from the theoretical value. Previous studies indicated that the structural hydration layer existing on the particle's surface could behave like a cushion to prevent particles colliding (Elimelech and O'Melia, 1990). Furthermore, the effects of structural hydration layer on the aggregation rate coefficient would be enhanced if the thickness ratio of hydration layer to the particle size increased (Kobayashi et al., 2005). Consequently, due to the smaller size of nanoparticles, the effect of structural hydration layer is obvious, leading to the larger deviation from the theoretical value. As the particle size increases, the influence of structural hydration layer gradually decreases, as a result, the fast aggregation rate coefficient is basically unchanged. As for the appropriate initial particle concentration, the value of the coefficient can be observed to be consistent with the theoretical value.

2.2. *Unique aggregation mechanism of nanoparticles with smaller size*

To clarify the phenomena mentioned above and to explore the aggregation mechanism of nanoparticles, the short-range structural hydration layer repulsive force was incorporated to the modified Smoluchowski theory (Fuchs, 1934) in this section. The conjecture of structural hydration layer on particles'

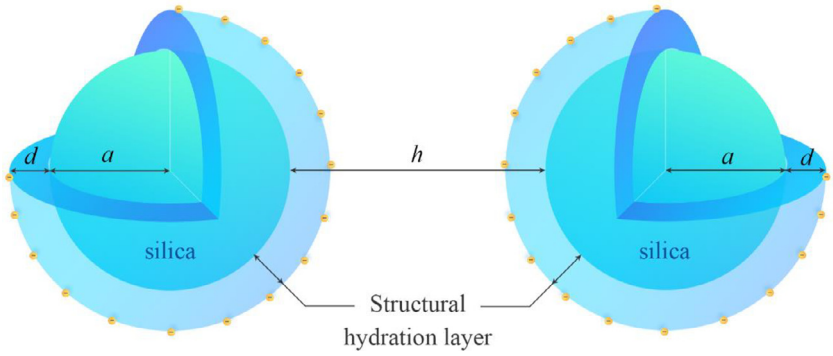

Fig. 3 – Schematics of the hypothesis of structural hydration layer. Solid sphere: silica; light blue annulus: structural hydration layer. The surface potential originated on the structural hydration layer and water interface. *a*, *d*, and *h* refer to the radius of particles, the thickness of structural hydration layer and the separation distance between particle surfaces, respectively.

surface was shown in Fig. 3. In the schematic, a (m) is the radius of particles, h (m) is the separation distance between particle surfaces and d (m) the thickness of structural hydration layer. The new formula for calculating the aggregation rate coefficient is shown below.

$$K = \frac{2k_BT}{\int_{2d}^{\infty} 3\mu a \frac{\beta(h-2d)\exp\left((V_A(h)+V_R(h-2d)+V_S(h))/k_BT\right)}{(2a+h)^2} dh} \times \left(1-\exp\left(\frac{V_{Tmin}}{k_BT}\right)\right) \quad (2)$$

where k_B (J/K) is the Boltzmann constant, T (K) is the absolute temperature, μ (Pa·sec) is the dynamic viscosity of water, $\beta(h\text{-}2d)$, h, $V_A(h)$, $V_R(h\text{-}2d)$, $V_S(h)$, a, d, and V_{Tmin} (J) refer to squeezing flow coefficient, the separation distance between particle surfaces, van der Waals (vdW) attraction, electrostatic repulsion, structural hydration layer repulsion, the radius of particles, the thickness of structural hydration layer and the minimum value of the total force between two particles, respectively. Considering the repulsive nature of structural hydration layer, the depth of the primary minimum would be so shallow that re-dispersion of small particles might occur, leading to the decrease of fast aggregation rate coefficient. Therefore, a coefficient (1-exp ($V_{Tmin}/(k_BT)$)) is introduced to modify the effect of re-dispersion (Richmond and Smith, 1975).

$\beta(h\text{-}2d)$ is the coefficient for the effect of squeezing flow between colliding particles. Reports stated that the structural hydration layer behaved like a rubber (Donose et al., 2005; Škvarla, 2013), therefore it's plausible to assume that the fluid flow cannot penetrate into the layer of $h < 2d$. The expression is shown as Eq. (3) (Honig et al., 1971).

$$\beta(h-2d) = \frac{6(h-2d)^2 + 13a(h-2d) + 2a^2}{6(h-2d)^2 + 4a(h-2d)} \quad (3)$$

The interaction forces between particles consist of three parts: vdW attraction $V_A(h)$ (J), electrostatic repulsion $V_R(h\text{-}2d)$ (J) and structural hydration layer repulsion $V_S(h)$ (J). The surface potential is assumed to originate on the water and structural hydration layer interfaces rather than the silica and structural hydration layer interfaces. Therefore, V_A is on the h scale, while V_R is on the $h\text{-}2d$ scale. The expressions are shown as follows (Hamaker, 1937; Škvarla, 2013):

$$V_A(h) = -\frac{A}{6}\left(\frac{2a^2}{h^2+4ah} + \frac{2a^2}{(h+2a)^2} + \ln\left(\frac{h^2+4ah}{(h+2a)^2}\right)\right) \quad (4)$$

where A (J) is the Hamaker constant, and the value of A is taken as 8.3×10^{-21} J for silica particles in water (Higashitani et al., 2017).

$$V_R(h-2d) = 2\pi\varepsilon_0\varepsilon_r a\varphi_0^2 \ln\left(1+\exp\left(-\kappa(h-2d)\right)\right) \quad (5)$$

$$\kappa = \sqrt{\frac{1000e^2N_A\sum_i Z_i^2M_i}{\varepsilon_0\varepsilon_r k_BT}} \quad (6)$$

where ε_0 (F/m) is the dielectric constant of free space, ε_r is the relative permittivity of the solution, φ_0 (V) is the surface potential which is usually replaced by zeta potential and κ (m^{-1}) is the inverse Debye screening length of diffuse layer around the spherical particles in the electrolyte solution. In Eq. (6), e (C) is the elementary electron charge, N_A (mol^{-1}) is Avogadro's number, Z_i is ion valence and M_i (mol/L) is electrolyte molarity.

$$V_S = \pi a\lambda V_0 \exp\left(-h/\lambda\right) \quad (7)$$

where V_0 (J/m^2) and λ (m) are arbitrary fitting parameters. Here $V_0 = 2$ mJ/m^2 and $\lambda = 0.45$ nm were used.

The revised model described aggregation behavior of nanoparticles with different particle size well, as shown in Fig. 2 (the carmine line). Through the model, the thickness of structure hydration layer under different conditions was obtained and two distinct features can be observed (Table 1): (1) the thickness of structural hydration layer was 11 nm for 130 nm particle, which was decreased to 5 nm for 190 nm particle. For particles with diameters larger than 190 nm, the thickness of structural hydration layer approaches a constant (4.5 nm for the 480 nm particle). This result indicated that the effect of particle size on aggregation behavior of nanoparticles was essentially due to the different thickness of structural hydration layer. As far as the authors know, this is the first time to quantitatively propose the thickness of structural hydration layer with different particle sizes. It was noticeable that

Table 1 – Experimental conditions and the results of calculation deduced by fitting with experimental data.

Particle size (nm)	Fast aggregation rate coefficient (m^3/sec)	Thickness of structural hydration layer (nm)	Distance at primary minimum (nm)
130	3.64×10^{-19}	11.0	22
140	5.22×10^{-19}	8.5	17
150	7.50×10^{-19}	7.5	15
160	9.44×10^{-19}	6.5	13
190	1.57×10^{-18}	5.0	10
270	1.61×10^{-18}	5.6	13
330	2.09×10^{-18}	5.6	13
480	3.21×10^{-18}	4.5	11

the thickness estimated (4.5–11 nm) was in accordance with that proposed by Bitter et al. (2013) (5–10 nm), who used total internal reflection microscopy to obtain the potential energy profile of silica at pH 10, which indicated that the thickness of structural hydration layer proposed in this study had credibility. (2) For particles with diameters less than 190 nm, distance at the primary minimum was exactly twice the thickness of structural hydration layer, while that of the particles larger than 190 nm was more than twice. Coincidently, 190 nm was also the inflection particle size, whose fast aggregation rate coefficient began to deviate from the theoretical value. This observation revealed that although nanoparticles with different particle sizes all have structural hydration layer on surfaces, only when the structural hydration layer thickness was exactly half of the distance at primary minimum, nanoparticles aggregation behavior would be affected obviously by structural hydration force. However, in the model proposed by Higashitani et al. (2017), the thickness of structural hydration layer was acquiescent as half of the distance at primary minimum, indicating that the model proposed in this study was more applicable and accurate.

2.3. *Effect of cation species on fast aggregation rate coefficients*

To further investigate the impact of structural hydration layer on different particle sizes under various conditions, nano-silica particles of diameter 130 and 270 nm, which was less and greater than the critical diameter 190 nm noted in Section 2.1, were selected for the detailed experiments. Literature results demonstrated that the charge and polarizability of the interface and surrounding ions, ion valences and concentration all played important roles in determining the nature and magnitude of structural hydration layer (Pashley, 1981). Therefore, the aggregation rate coefficients at different concentrations of electrolytes with different cations were investigated and the results were shown in Fig. 4.

For 270 nm silica particles, the dependence of ionic strength on aggregation rate coefficients conformed with the DLVO theory (Fig. 4a) and the fast aggregation rate coefficients of nano-silica particles in presence of three electrolytes were almost the same when the electrolytes concentration reached the CCC. Additionally, the CCC of NaCl, $BaCl_2$ and $LaCl_3$ were 1000, 10 and 2 mmol/L, respectively, suggesting multivalent cations were more effective than monovalent cations in screening the charge on nanoparticles. The CCC for

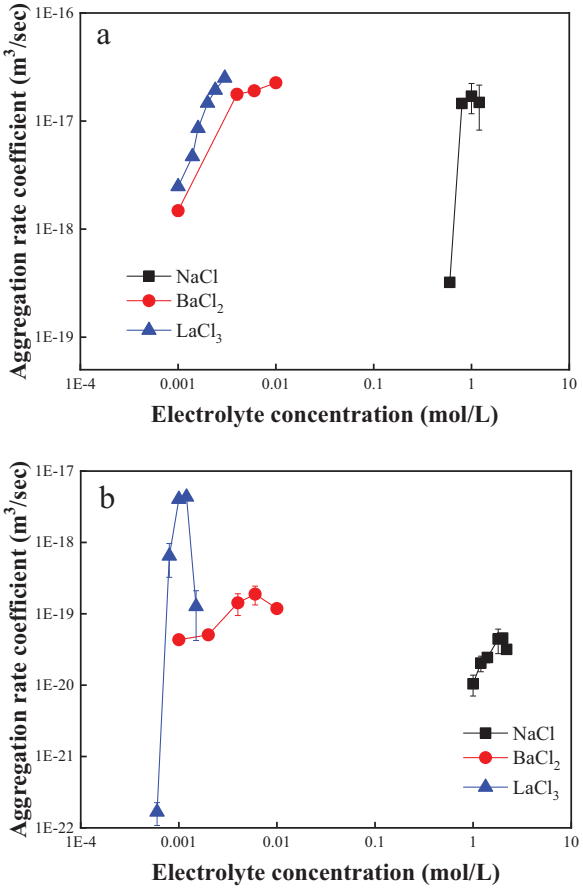

Fig. 4 – Aggregation rate coefficient as a function of electrolyte concentration and valence at pH 10 and 2.40 × 10^{17} particles/m^3 initial particle concentration. (a) Diameter 270 nm; (b) diameter 130 nm.

ions with different valences were proportional to z^{-6} to z^{-2} (z is the cation valence), following Schulze-Hardy rule (Cao et al., 2015).

Comparison between Fig. 4a and b demonstrated the following distinct aggregation kinetics characteristics for the smaller particles (130 nm): (1) the change of aggregation rate coefficients with ionic strength did not accord with DLVO theory. As the ionic strength further increased, aggregation rate coefficients were decreased rather than remaining con-

Table 2 – Hydrated radius and hydration Gibbs free energy of cations.

Cation	Hydrated radius (Å)	Hydration Gibbs free energy (kJ/mol)
Na^+	3.58	−365
Ba^{2+}	4.04	−1250
La^{3+}	4.52	−3145

stant; (2) For the three kinds of electrolytes, the fast aggregation rate coefficients were different, the order was $LaCl_3$ > $BaCl_2$ > NaCl. The former difference was because structural hydration repulsion between nanoparticles was more obvious at high ionic strength. Several reports also discovered the same phenomenon. For instance, Elimelech (1990) found that the attachment efficiency of 46 nm latex particles exhibited a maximum at 10 mmol/L $CaCl_2$, while as the concentration was larger than 10 mmol/L, the attachment efficiency decreased, indicating an apparent increase of repulsion with ionic strength. Healy et al. (1978) also proposed that the increased ionic strength enhanced the repulsion forces by the structural hydration layer so the aggregate rate coefficient was reduced. If two particles can approach each other by screening off the long-range electrostatic interaction using high ionic strength, then the repulsive interactions between structural hydration layers on the two particles surfaces can be predominant to limit aggregation (Bitter et al., 2013). As shown in Table 2 (Marcus, 1994; Nightingale, 1959), the hydrated radii and hydration Gibbs free energy of three cations follow the order of La^{3+} > Ba^{2+} > Na^+. However, the structural hydration layer thickness for 2 mol/L NaCl, 10 mmol/L $BaCl_2$ and 1.5 mmol/L $LaCl_3$ were calculated as 32, 10 and 5 nm, respectively, in the order of La^{3+} < Ba^{2+} < Na^+. Consequently, the influence of cation species on fast aggregation rate coefficient was the result of synergistic effect of ionic physical properties and ionic strength (Xu et al., 2019), resulting in the various fast aggregation rate coefficients.

2.4. *Effects of solution pH on fast aggregation rate coefficients*

According to the DLVO theory, when the pH is higher than the point of zero charge (PZC), increasing pH value would make the particle surface more negative so the aggregation rate coefficient would drop. Conversely, Higashitani et al. (1990) and this study observed no aggregation for nano-silica particles (with a PZC at around 2-3) at pH inferior to 9. Similar finding has also been discovered by Kobayashi et al. (2005) that no aggregation could be detected at pH inferior to 6. The discrepancy may be caused by the different size and surface properties of the silica used. The stronger repulsion at lower pH could be attributed to the adsorption of hydroxyls onto the particle surface. As in the lower pH, the silanol groups on silica surface could be so hydrophilic that it formed a thick structural layer of adsorbed water molecules (Iler, 1979). When pH was above 9, the dissociation of silanol groups reduced the thickness of the structural hydration layer, so aggregation could occur.

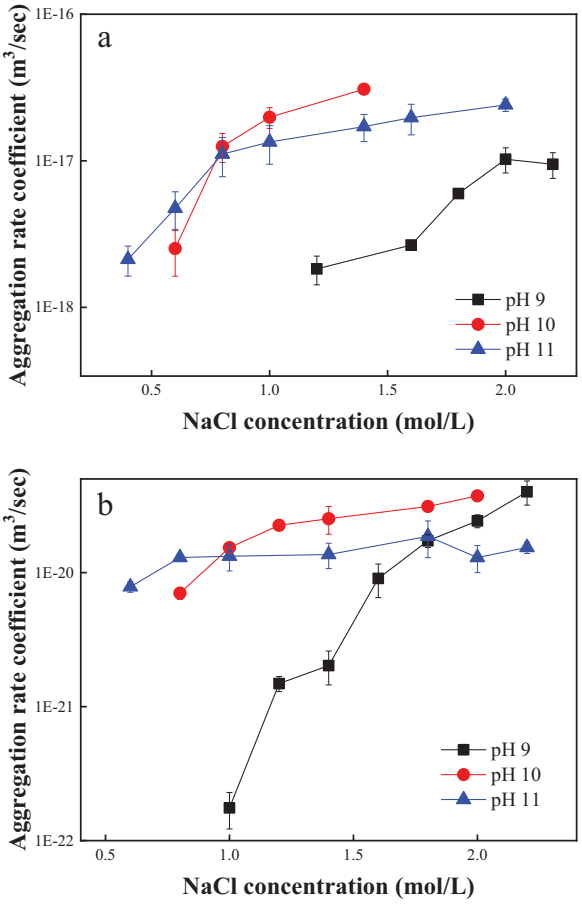

Fig. 5 – Aggregation rate coefficient as a function of NaCl concentration and pH with the initial particle concentration of 1.85 x 10^{17} particles/m^3. (a) Diameter 270 nm; (b) diameter 130 nm.

To further investigate the influence of pH on aggregation behavior of nanoparticles with different particle size, measurements were carried out at different alkaline conditions, as shown in Fig. 5. By comparing nano-silica particles' aggregation rate coefficients with diameter 270 nm (Fig. 5a) and 130 nm (Fig. 5b), a few differences were observed: (1) as noted in previous section, the fast aggregation rate coefficients of nanoparticle with 130 nm diameter were lower than those with 270 nm diameter; (2) the fast aggregation rate coefficient was slightly increased with pH value, especially for the 270 nm silica. As shown in Fig. S4, the zeta potentials of 270 nm silica at pH 9 were higher than those at pH 10 and 11 in the diffusion-controlled regime, while the zeta potentials of 130 nm silica were almost the same under the three pH values, which was not consistent with the change of fast aggregation rate coefficients, indicating that electrostatic repulsion was not dominant. Therefore, the deprotonation degree of silanol groups on silica surfaces would be enhanced to make surface more hydrophobic when the solution became more alkaline, corresponding to the noted promotion of aggregation rate coefficients. The differences between 270 and 130 nm particles can also be successfully interpreted by the theory that the ac-

tion of structural hydration layer was stronger for the smaller nanoparticles.

One interesting finding was that, regardless of the particle size, the fast aggregation rate coefficients at pH 11 were lower than those at pH 10. The zeta potentials for 270 and 130 nm silica in the diffusion-controlled regime at pH 10 were not significant different with those at pH 11 (Fig. S4), which indicated that the impact of electrostatic repulsion could be excluded. Then there were two possible mechanisms can correspond to the difference of fast aggregation rate coefficients. The first was the dissolution of silica. Previous studies indicated that silica would rapidly dissolve in solutions of high pH, causing gel-like layers form covered with re-precipitated polysilicic acid chains (Iler, 1979; Tanaka and Takahashi, 1999). The short flexible polymer-like segments of polysilicic acid chains anchored to the surface. A mathematical model was proposed for the swelling degree of polymer in 1991, which predicted that as long as the pH of external solution was higher than the dissociation constant of ionizable groups on the polyelectrolyte, a sharp increase in swelling would occur (Brannon-Peppas and Peppas, 1991). Similarly, when solution pH exceeded the dissociation constant of silanol groups on silica surface ($pK_{a1} = 9.77$) (Iler, 1979), the structural hydration layer would swell. The calculated results of structural hydration layer thickness also verified the conjecture. For 130 nm nanosilica, when the concentration was 2 mol/L NaCl, the thickness of structural hydration layer at pH 11 was 11 nm thicker than that at pH 10. Another possible mechanism was the formation of hydrogen bonding. McNamee and Higashitani (2015) applied AFM to detect the surface force of silica particles and found that the adhesion force was increased distinctly in alkaline solution. Moreover, Fuji et al. (1999) revealed that hydrogen bonding was the dominant component of the adhesion force between silica surfaces with a high silanol density. Therefore, it can be assumed that at high pH, hydrogen bonds between hydroxyls and silanols on the silica surface would form, whose formation weaken the role of vdW attraction and increased the energy barrier between particles, resulting in a decrease of fast aggregation rate coefficient.

According to the above experiments, the formation mechanism of structural hydration layer is water molecules or hydrated counterions adsorption. For the nanoparticles with smaller size, ionic strength, ionic valence and pH can influence the thickness of structural hydration layer, resulting in the change of fast aggregation rate coefficient. The results in Sections 2.3 and 2.4 proved the applicability and feasibility of the model proposed in Section 2.2.

2.5. *Implementation to practice*

Based on this study, the unique aggregation mechanism of nanoparticles with smaller size is that the structural hydration force is dominant. Due to the higher stability, longer migration distance and easier to be captured by organisms, nanoparticles with smaller size have higher potential risks to aquatic environments. Previous researches discovered not only most natural minerals, but also biological materials such as lipid bilayers, DNA, humic acid and protein all have structural hydration layer on the surfaces (Kuchuk and Sivan, 2018; Pattni and Heyden, 2019; Stachura et al., 2019; Xu et al., 2019). Therefore, the formation mechanism of structural hydration layer and the influence of which on nanoparticles with different particle size were investigated in this study, which provided the theoretical foundation for predicting and assessing the fate and risk of biological materials in aquatic environments.

In addition, specific treatments can be designed to remove nanoparticles with structural hydration layer. For instance, in the traditional coagulation treatment, different coagulants are added to make particles cross the energy barrier and aggregate at the primary minimum. While due to the domination of structural hydration layer repulsion for nanoparticles, the values of the secondary energy minimum are small (Zhang et al., 2012), which makes it possible for the nanoparticles successfully aggregate at the secondary minimum by reducing the hydrodynamic shear rate with smaller amount of coagulant (Wang et al., 2019). What's more, flotation treatment of nanoparticles is limited because of the low probability collision of nanoparticles and bubbles (Zhang and Guiraud, 2017). Since the structural hydration layer is hydrophilic, adding surfacant to modify the surface of bubbles to be hydrophilic can achieve efficient removal of nanoparticles.

3. Conclusions

This study systematically investigated the influence of particle size on the aggregation behavior of nanoparticles under different initial particle concentration, solution pH, ionic strength and ionic valence. The DLVO theory can well describe the fast aggregation rate coefficients of nanoparticles with larger than 190 nm diameter at appropriate initial particle concentration. Whereas the fast aggregation rate coefficients of nanoparticles with smaller than 190 nm diameter were obviously lower than the theoretical value. Through the revised model, it is found that the reason for anomalous aggregation behavior was the different structural hydration layer thickness on the surfaces of nanoparticles with various sizes. The thickness gradually decreased from 11 nm for 130 nm nanoparticles to 5.0 nm for 190 nm nanoparticles, and then approached a plateau 4.5 nm as the particle diameter was further increased. Only when the distance at primary minimum was exactly twice the thickness of structural hydration layer, the structural hydration repulsive force would dominate, leading to higher stability of nanoparticles. Ionic strength, cation species and pH all played important roles in determining the nature and magnitude of structural hydration layer, which indicated the formation mechanism of structural hydration layer was water molecules or hydrated counterions adsorption. This study provided a deeper understanding of the aggregation mechanisms operating at nanoscale and the characteristics of the structural hydration layer. Furthermore, the theoretical foundation could offer a valuable reference to assess the fate, risk and specific treatment of nanoparticles in aquatic environments.

Declaration of competing interest

There are no conflicts of interest to declare.

Acknowledgments

This work was supported by the National Natural Science Foundation of China (Nos. 51808530 and 51778604).

Appendix A. Supplementary data

Supplementary material associated with this article can be found in the online version at doi:10.1016/j.jes.2020.10.007.

REFERENCES

Adachi, Y., Stuart, M.A.C., Fokkink, R., 1994. Kinetics of turbulent coagulation studied by means of end-over-end rotation. J. Colloid Interf. Sci. 165, 310–317.
Adachi, Y., 1995. Dynamic aspects of coagulation flocculation. Adv. Colloid Interf. Sci. 56, 1–31.
Adeleye, A.S., Pokhrel, S., Madler, L., Keller, A.A., 2018. Influence of nanoparticle doping on the colloidal stability and toxicity of copper oxide nanoparticles in synthetic and natural waters. Water Res. 132, 12–22.
Bitter, J.L., Duncan, G.A., Beltran-Villegas, D.J., Fairbrother, D.H., Bevan, M.A., 2013. Anomalous silica colloid stability and gel layer mediated interactions. Langmuir 29, 8835–8844.
Brannon-Peppas, L., Peppas, N.A., 1991. Equilibrium swelling behavior of pH-sensitive hydrogels. Chem. Eng. Sci. 46, 715–722.
Cao, T., Szilagyi, I., Oncsik, T., Borkovec, M., Trefalt, G., 2015. Aggregation of colloidal particles in the presence of multivalent co-ions: the inverse Schulze-Hardy rule. Langmuir 31, 6610–6614.
Chekli, L., Phuntsho, S., Roy, M., Lombi, E., Donner, E., Shon, H.K., 2013. Assessing the aggregation behaviour of iron oxide nanoparticles under relevant environmental conditions using a multi-method approach. Water Res. 47, 4585–4599.
Combarros, R.G., Collado, S., Diaz, M., 2016. Toxicity of titanium dioxide nanoparticles on Pseudomonas putida. Water Res. 90, 378–386.
Derjaguin, B.V., 1940. On the repulsive forces between charged colloid particles and on the theory of slow coagulation and stability of lyophobic sols. Trans. Faraday Soc. 36, 203–215.
Derjaguin, B.V., Landau, L.D., 1941. Theory of the stability of strongly charged lyophobic sols and of the adhesion of strongly charged particles in solutions of electrolytes. Acta Physicochim. USSR 14, 633–662.
Donose, B.C., Vakarelski, I.U., Higashitani, K., 2005. Silica surfaces lubrication by hydrated cations adsorption from electrolyte solutions. Langmuir 21, 1834–1839.
Elimelech, M.J., 1990. Indirect evidence for hydration forces in the deposition of polystyrene latex colloids on glass surfaces. J. Chem. Soc. Faraday Trans. 86, 1623–1624.
Elimelech, M., O'Melia, C.R., 1990. Kinetics of deposition of colloidal particles in porous media. Environ. Sci. Technol. 24, 1528–1536.
French, R.A., Jacobson, A.R., Kim, B., Isley, S.L., Penn, R.L., Baveye, P.C., 2009. Influence of ionic strength, pH, and cation valence on aggregation kinetics of Titanium dioxide nanoparticles. Environ. Sci. Technol. 43, 1354–1359.
Fuchs, N., 1934. Zur theorie der koagulation. Z. Phys. Chem., Abt. A 171, 199–208.
Fuji, M., Machida, K., Takei, T., Watanabe, T., Chikazawa, N., 1999. Effect of wettability on adhesion force between silica particles evaluated by atomic force microscopy measurement as a function of relative humidity. Langmuir 15, 4584–4589.
Hamaker, H.C., 1937. The London-van der Waals attraction between spherical particles. Physica 4, 1058–1072.
Hatton, W., McFadyen, P., Smith, A.L., 1974. Rapid flocculation rates of polystyrene latex dispersions. J. Chem. Soc. Faraday Trans. 1 70, 655–660.
Healy, T.W., Homola, A., James, R.O., 1978. Coagulation of amphoteric latex colloids: reversibility and specific ion effects. Faraday Discuss. Chem. Soc. 65, 527–536.
Higashitani, K., Kondo, M., Hatade, S., 1990. Effect of particle size on coagulation rate of ultrafine colloidal particles. J. Colloid Interf. Sci. 142, 204–212.
Higashitani, K., Nakamura, K., Shimamura, T., Fukasawa, T., Tsuchiya, K., Mori, Y., 2017. Orders of magnitude reduction of rapid coagulation rate with decreasing size of silica nanoparticles. Langmuir 33, 5046–5051.
Holthoff, H., Egelhaaf, S.U., Borkovec, M., Schurtenberger, P., Sticher, H., 1996. Coagulation rate measurements of colloidal particles by simultaneous static and dynamic light scattering. Langmuir 12, 5541–5549.
Honig, E.P., Roebersen, G.J., Wiersema, P.H., 1971. Effect of hydrodynamic interaction on the coagulation rate of hydrophobic colloids. J. Colloid Interf. Sci. 36, 97–109.
Iler, R.K. (Ed.), 1979. The Chemistry of Silica. Wiley, New York.
Ivanić, M., Durn, G., Škapin, S.D., Sondi, I., 2020. Size-related mineralogical and surface physicochemical properties of the mineral particles from the recent sediments of the Eastern Adriatic sea. Chemosphere 249, 126531.
Jarvis, P., Jefferson, B., Gregory, J., Parsons, S.A., 2005. A review of floc strength and breakage. Water Res. 39, 3121–3137.
Kansara, K., Paruthi, A., Misra, S.K., Karakoti, A.S., Kumar, A., 2019. Montmorillonite clay and humic acid modulate the behavior of copper oxide nanoparticles in aqueous environment and induces developmental defects in zebrafish embryo. Environ. Pollut. 255 (Part 2), 113313.
Kilpatrick, J.I., Loh, S.H., Jarvis, S.P., 2013. Directly probing the effects of ions on hydration forces at interfaces. J. Am. Chem. Soc. 135, 2628–2634.
Kobayashi, M., Juillerat, F., Galletto, P., Bowen, P., Borkovec, M., 2005. Aggregation and charging of colloidal silica particles: effect of particle size. Langmuir 21, 5761–5769.
Kuchuk, K., Sivan, U., 2018. Hydration structure of a single DNA molecule revealed by frequency-modulation atomic force microscopy. Nano Lett. 18, 2733–2737.
Lips, A., Willis, E., 1973. Low angle light scattering technique for the study of coagulation. J. Chem. Soc., Faraday Trans. 1 69, 1226–1236.
Lish, R.A.D., Johari, S.A., Sarkheil, M., Yu, J.I., 2019. On how environmental and experimental conditions affect the results of aquatic nanotoxicology on brine shrimp (Artemia salina): a case of silver nanoparticles toxicity. Environ. Pollut. 255 (Part 3), 113358.
Liu, X., Wazne, M., Chou, T., Xiao, R., Xu, S., 2011. Influence of Ca^{2+} and Suwannee river humic acid on aggregation of silicon nanoparticles in aqueous media. Water Res. 45, 105–112.
Liu, Y., Yang, T., Wang, L., Huang, Z., Li, J., Cheng, H., et al., 2018. Interpreting the effects of natural organic matter on antimicrobial activity of Ag_2S nanoparticles with soft particle theory. Water Res. 145, 12–20.
Liu, S., Cui, M., Li, X., Thuyet, D.Q., Fan, W., 2019. Effects of hydrophobicity of titanium dioxide nanoparticles and exposure scenarios on copper uptake and toxicity in Daphnia magna. Water Res. 154, 162–170.
Marcus, Y., 1994. A simple empirical model describing the thermodynamics of hydration of ions of widely varying charges, sizes, and shapes. Biophys. Chem. 51, 111–127.
McNamee, C.E., Higashitani, K., 2015. Time dependence of silica surfaces on their interactions in water and alkaline solutions. Langmuir 31, 6064–6071.

Miyahara, K., Adachi, Y., Nakaishi, K., Ohtsubo, M., 2002. Settling velocity of a sodium montmorillonite floc under high ionic strength. Colloids Surf. A Physicochem. Eng. Asp. 196, 87–91.
Nightingale, E.R., 1959. Phenomenological theory of ion solvation - effective radii of hydrated ions. J. Phys. Chem. 63, 1381–1387.
Pashley, R.M., 1981. DLVO and hydration forces between mica surfaces in Li^+, Na^+, K^+, and Cs^+ electrolyte solutions: a correlation of double-layer and hydration forces with surface cation exchange properties. J. Colloid Interf. Sci. 83, 531–546.
Pattni, V., Heyden, M., 2019. Pressure effects on protein hydration water thermodynamics. J. Phys. Chem. B 123, 6014–6022.
Reischl, B., Raiteri, P., Gale, J.D., Rohl, A.L., 2019. Atomistic simulation of atomic force microscopy imaging of hydration layers on calcite, dolomite, and magnesite surfaces. J. Phys. Chem. C 123, 14985–14992.
Richmond, P., Smith, A.L., 1975. Initial rate constants for coagulation in the presence of energy minima of restricted depth. J. Chem. Soc. Faraday Trans. 2 71, 468–473.
Russel, W.B., Saville, D.A., Schowalter, W.R. (Eds.), 1989. Colloidal Dispersions. Cambridge University Press, New York.
Škvarla, J., 2013. Quantitative interpretation of anomalous coagulation behavior of colloidal silica using a swellable polyelectrolyte gel model of electrical double layer. Langmuir 29, 8809–8824.
Spielman, L.A., 1970. Viscous interactions in Brownian coagulation. J. Colloid Interf. Sci. 33, 562–571.
Stachura, S.S., Malajczuk, C.J., Mancera, R.L., 2019. Does sucrose change its mechanism of stabilization of lipid bilayers during desiccation? Influences of hydration and concentration. Langmuir 35, 15389–15400.
Sun, H.Y., Jiao, R.Y., Xu, H., An, G.Y., Wang, D.S., 2019. The influence of particle size and concentration combined with pH on coagulation mechanisms. J. Environ. Sci. 82, 39–46.
Tanaka, M., Takahashi, K., 1999. The identification of chemical species of silica in sodium hydroxide, potassium hydroxide and sodium chloride solutions by FAB-MS. Anal. Sci. 15, 1241–1250.
Verwey, E.J., Overbeek, J.Th.G. (Eds.), 1948. Theory of the Stability of Lyophobic Colloids. Elsevier, Amsterdam.
Von Smoluchowski, M.Z., 1917. Versuch einer mathematischen theorie der koagulationskinetik kolloider Lösungen. Phys. Chem. (Munich) 92, 129.
Wang, X., Adeleye, A.S., Wang, H., Zhang, M., Liu, M., Wang, Y., et al., 2018. Interactions between polybrominated diphenyl ethers (PBDEs) and TiO_2 nanoparticle in artificial and natural waters. Water Res. 146, 98–108.
Wang, H., Zhang, W., Zeng, S., Shen, C., Jin, C., Huang, Y., 2019. Interactions between nanoparticles and fractal surfaces. Water Res. 151, 296–309.
Wang, J., Zhao, X., Wu, A., Tang, Z., Niu, L., Wu, F., et al., 2020. Aggregation and stability of sulfate-modified polystyrene nanoplastics in synthetic and natural waters. Environ. Pollut., 114240 doi:10.1016/j.envpol.2020.114240.
Xu, F., Yao, Y., Alvarez, P.J.J., Li, Q., Fu, H., Yin, D., et al., 2019. Specific ion effects on the aggregation behavior of aquatic natural organic matter. J. Colloid Interf. Sci. 556, 734–742.
Yan, C., Cheng, T., Shang, J., 2019. Effect of bovine serum albumin on stability and transport of kaolinite colloid. Water Res. 155, 204–213.
Zaouri, N., Gutierrez, L., Dramas, L., Garces, D., Croue, J.P., 2017. Interfacial interactions between Skeletonema costatum extracellular organic matter and metal oxides: implications for ceramic membrane filtration. Water Res. 116, 194–202.
Zhang, W., Yao, Y., Sullivan, N., Chen, Y.S., 2011. Modeling the primary size effects of citrate-coated silver nanoparticles on their ion release kinetics. Environ. Sci. Technol. 45, 4422–4428.
Zhang, W., Crittenden, J., Li, K., Chen, Y., 2012. Attachment efficiency of nanoparticle aggregation in aqueous dispersions: modeling and experimental validation. Environ. Sci. Technol. 46, 7054–7062.
Zhang, W., Rattanaudompol, U-sa., Li, H, Bouchard, D., 2013. Effects of humic and fulvic acids on aggregation of aqu/nC60 nanoparticles. Water Res. 47 (5), 1793–1802.
Zhang, M., Guiraud, P., 2017. Surface-modified microbubbles (colloidal gas aphrons) for nanoparticle removal in a continuous bubble generation-flotation separation system. Water Res. 126, 399–410.
Zhang, M., Wang, X., Du, T., Wang, H., Hao, H., Wang, Y., et al., 2019. Effects of carbon materials on the formation of disinfection byproducts during chlorination: pore structure and functional groups. Water Res. 162, 1–10.
Zhang, Y.Y., Luo, Y.Y., Guo, X.T., Xia, T.J., Wang, T.C., Jia, H.Z., et al., 2020. Charge mediated interaction of polystyrene nanoplastic (PSNP) with minerals in aqueous phase. Water Res. 178, 115861. doi:10.1016/j.watres.2020.115861.
Zhou, H., Xu, S., Mi, L., Sun, Z., Qin, Y., 2014. Study on independently using static and dynamic light scattering methods to determine the coagulation rate. J. Chem. Phys. 141, 094302.